Existence of an optimized stellarator with simple coils

Guodong Yu, Zhichen Feng ⓘ**, Peiyou Jiang and GuoYong Fu** ⓘ**,†**

Institute for Fusion Theory and Simulation and School of Physics, Zhejiang University,
Hangzhou 310027, PR China

An optimized compact stellarator with four simple coils is obtained from direct optimization via a coil shape. The new stellarator consists of two interlocking coils and two vertical field coils similar to those of the Columbia Non-neutral Torus (CNT) (Pedersen *et al.*, *Phys. Rev. Lett.*, vol. 88, 2002, pp. 205002). The optimized configuration has a global magnetic well and a low helical ripple level comparable to that of Wendelstein 7-X (W7-X) (Wolf *et al.*, *Nucl. Fusion*, vol. 57, 2017, pp. 102020). The two interlocking coils have a smooth three-dimensional shape much simpler than those of advanced stellarators such as W7-X. This result opens up possibilities of future stellarator reactors with simplified coils.

Key words: fusion plasma, plasma confinement, plasma devices

---

1. Introduction

The two main approaches of magnetic confinement fusion (MCF) are tokamaks and stellarators. The tokamak is currently the dominant approach with advantages of axisymmetric geometry and achieved plasma parameters significantly better than those of other MCF devices. However, stellarators have recently enjoyed a renaissance as recent results of the advanced stellarator Wendelstein 7-X (W7-X) (Wolf *et al.* 2017) demonstrated a reduced neoclassical energy transport (Dinklage *et al.* 2018; Beidler *et al.* 2021). It is expected that the plasma performance of W7-X can reach a level comparable to that of an equivalent tokamak in the next few years. Stellarators have advantages of naturally steady-state operations because their magnetic fields are mainly generated by external coils and plasma current is not needed for confinement and is usually quite small. The harmful current-driven instabilities, such as disruptions in tokamaks, are absent in stellarators. The confinement properties of stellarator plasmas are largely determined by external coils. The recent success of W7-X demonstrates that it is possible to build an optimized three-dimensional (3-D) coil to such high precisions that the designed plasma

† Email address for correspondence: gyfu@zju.edu.cn

confinement performance can be achieved as predicted in actual experiments. It has been argued recently that the stellarator approach provides the fastest track to the realization of fusion energy because favourable plasma confinement properties can be designed, realized and controlled almost fully by external 3-D coils (Boozer 2021).

The advanced stellarators such as W7-X are usually designed for improved neoclassical confinement and magnetohydrodynamic (MHD) stability by the two-stage approach. First, the shape of the plasma boundary is varied to obtain optimized properties. Second, the optimized boundary shape is realized by designing the shapes of the 3-D coils. Unfortunately, the resulting 3-D coils are usually quite complex and are difficult and costly to build. This is evidenced by the long delay of the W7-X project (Riße 2009) and the cancellation of the NCSX project (Neilson *et al.* 2010) due to difficulties in engineering and building of the 3-D coils. Therefore, it is necessary to simplify the 3-D coils for the stellarator to become an economical platform for fusion reactors. For this reason, recently, coil simplification of the stellarator has been a subject of intensive studies including reducing coil complexity in the optimization (Lobsien, Drevlak & Pedersen 2018; Henneberg *et al.* 2021; Kruger *et al.* 2021) as well as using permanent magnets to replace 3-D coils (Helander *et al.* 2020; Zhu *et al.* 2020; Xu *et al.* 2021).

In this work, we explore the possibilities of optimized stellarators with simplified coils. We use a direct optimization method of varying the coil shape to optimize both plasma confinement and MHD stability. In this way, we can effectively control the complexity of coils while optimizing the plasma properties. The details of the optimization method will be given later. Following our recent work (Yu *et al.* 2021), we choose the coil topology of the Columbia Non-neutral Torus (CNT) (Pedersen *et al.* 2012) for our optimization space. The CNT consists of two circular interlocking (IL) coils and two circular vertical field (VF) coils. It is arguably the simplest compact stellarator ever built and successfully operated (Pedersen *et al.* 2012). Here we carry out a global optimization of both neoclassical confinement and MHD stability by varying the 3-D shape of the two IL coils. An initial phase of this work has been done recently by targeting only the neoclassical transport. The results showed that the effective helical ripple level was reduced by an order of magnitude as compared to that of the CNT indicating significant improvement in neoclassical confinement (Yu *et al.* 2021). This was realized by two planar IL coils with elliptical shape. In the present work, a much broader parameter space of coil shape is explored allowing a 3-D shape of the two IL coils. As a result, an optimized Compact Stellarator with Simple Coils (CSSC), to be called CSSC, has been discovered. CSSC has both a global magnetic well and a low level of helical ripple comparable to that of W7-X. This breakthrough opens up possibilities of stellarator reactors with simplified coils. The design of CSSC can be used as a basis for a low-cost experiment to study the physics of compact stellarators. The design could also be used as a candidate stellarator for electron–positron plasma experiments (Pedersen *et al.* 2012).

The paper is organized as follows. Section 2 describes the optimization results of CSSC. Section 3 describes the optimization method used in obtaining CSSC. Section 4 considers the effects of finite beta. Finally, conclusions of this work are given in Section 5.

2. Optimization results

We now describe the configuration specification and physics properties of CSSC in detail. The optimized configuration CSSC is obtained by targeting plasma volume, flux surface quality, rotational transform, neoclassical transport as well as MHD stability. In our optimization, the radius of the two circular VF coils is varied while the distance between them is fixed. The shapes of the two IL coils are varied and are described by the following

	Parameter	Range	Results
IL coil	$x_{c,0}$	$0.3 \sim 0.6$	0.509
	$x_{c,1}$	$0.6 \sim 1.2$	1.051
	$x_{c,2}$	$-0.3 \sim 0.3$	0.227
	$x_{c,3}$	$-0.1 \sim 0.1$	-2.622×10^{-2}
	$y_{s,1}$	$0.6 \sim 1.2$	0.806
	$y_{s,2}$	$-0.3 \sim 0.3$	0.162
	$y_{s,3}$	$-0.1 \sim 0.1$	-6.257×10^{-2}
	$z_{s,1}$	$-0.4 \sim 0.8$	0.667
	$z_{s,2}$	$-0.2 \sim 0.2$	-3.87×10^{-2}
	$z_{s,3}$	$-0.1 \sim 0.1$	-6.052×10^{-2}
VF coil	$y_{s,1} = x_{c,1}$	$1.0 \sim 2.0$	1.850
	$z_{c,0}$	0.77	0.770
Current ratio	I_{IL}/I_{VF}	$1 \sim 3$	1.323

TABLE 1. Optimization ranges of coil Fourier coefficients and coil current ratio, as well as the optimized results.

Fourier representation (Zhu *et al.* 2017):

$$\left.\begin{aligned} x &= x_{c,0} + \sum_{n=1}^{n_f} x_{c,n} \cos(nt), \\ y &= \sum_{n=1}^{n_f} y_{s,n} \sin(nt), \\ z &= \sum_{n=1}^{n_f} z_{s,n} \sin(nt), \end{aligned}\right\} \tag{2.1}$$

where (x, y, z) are Cartesian coordinates of line coils, t is an angle variable in a range of $[0, 2\pi]$ and n is the harmonic number. The total number of Fourier coefficients for each IL coil is $3 \times n_f + 1$ with n_f being the maximum harmonic number. To maintain two periods of flux surfaces, the two IL coils are constrained to have the same shape. Furthermore, $n_f = 3$ is chosen in this work. This choice of $n_f = 3$ is a compromise between allowing enough degrees of freedom while constraining the coil complexity. Finally, taking into account the current ratio between IL coils and VF coils, the optimization parameter space has a total of 12 degrees of freedom.

Table 1 shows the Fourier coefficients of the optimized configuration CSSC (fourth column) along with the optimization ranges for Fourier coefficients (third column).

Figure 1 shows the 3-D schematic of coils and the last closed flux surface (LCFS) of the CSSC. We observe that the two IL coils have a smooth shape with modest 3-D variation. The averaged radius of the IL coils is 1.11 m. The radius of the vertical field coils is 1.85 m. The distance between the two vertical field coils is 1.54 m. The current ratio of IL coils and VF coils is 1.323. The minor and major radius of the LCFS is 0.15 m and 0.58 m respectively, corresponding to a low aspect ratio of $R/a = 3.87$. The volume within LCFS is 0.27 m^3. The Poincaré plots of vacuum magnetic surfaces are shown in figure 2 at toroidal angles of $0°$ and $90°$. The configuration has good magnetic flux surfaces except for a small magnetic island at the $\iota = 0.25$ surface. The rotational transform profile is shown
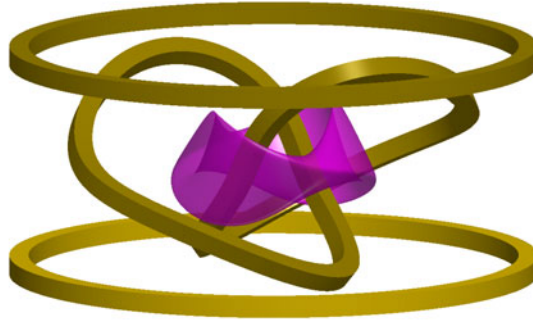
FIGURE 1. Optimized stellarator with four simple coils: the gold colour denotes the two inner interlocked 3-D coils located between two circular vertical field coils; the purple colour denotes the last closed flux surface.
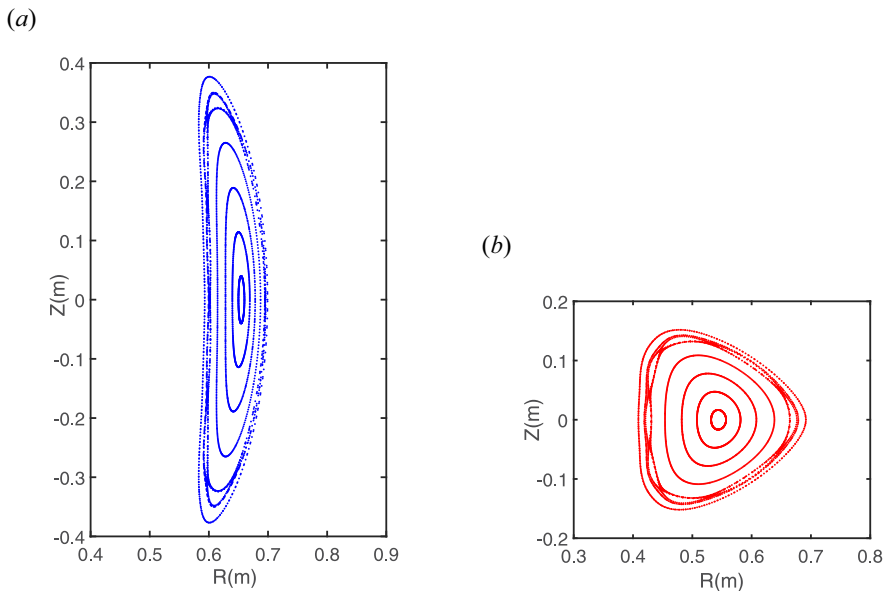
(*a*)

(*b*)

FIGURE 2. Poincaré plot of vacuum magnetic surfaces at toroidal angles: (*a*) $\phi = 0°$; (*b*) $\phi = 90°$.

in figure 3 and is seen to vary from 0.2 at the magnetic axis to 0.28 at the LCFS with modest magnetic shear.

One of our main optimization targets is neoclassical transport, particularly the so-called $1/\nu$ neoclassical transport with ν being the collision frequency of plasmas. This $1/\nu$ scaling is very unfavourable for stellarator confinement for the high-temperature regime of fusion plasmas because the transport increases strongly with plasma temperature (Ho & Kulsrud 1987). Therefore, the minimization of neoclassical transport in the $1/\nu$ regime is necessary for stellarator reactors. It has been shown that the $1/\nu$ transport is proportional the effective helical ripple coefficient $\epsilon_{\mathrm{eff}}^{3/2}$ (Nemov *et al.* 1999). We use this coefficient as a target for neoclassical transport. Figure 4 shows the radial profile of $\epsilon_{\mathrm{eff}}^{3/2}$ of CSSC as well
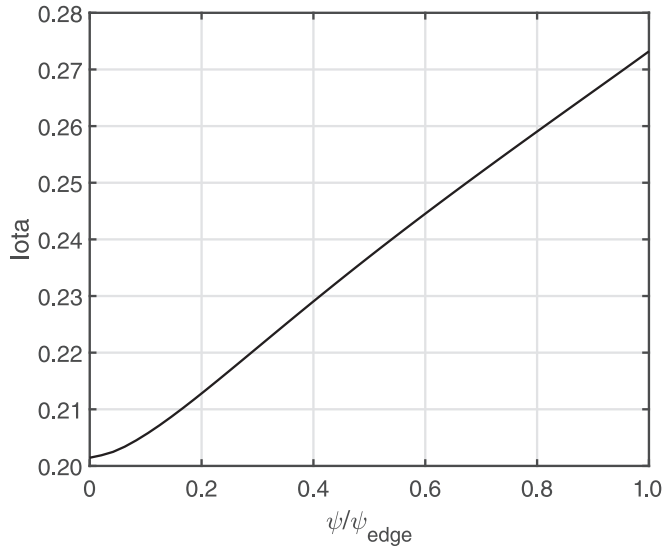
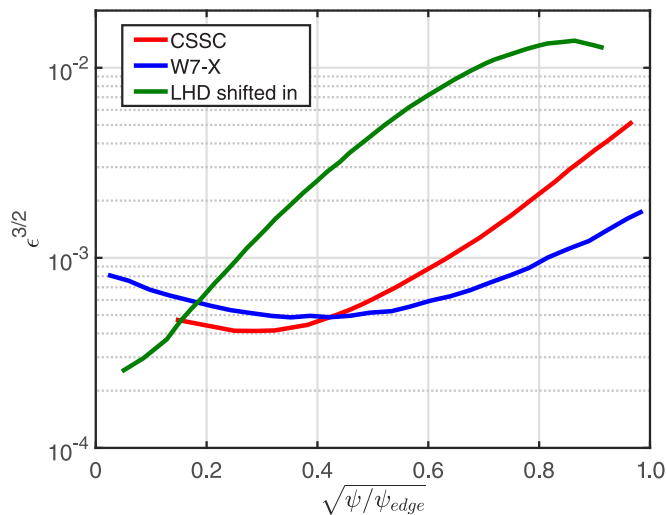FIGURE 3. Rotational transform iota versus normalized toroidal flux.

FIGURE 4. Effective helical ripple $\epsilon_{\text{eff}}^{3/2}$ versus square root of the normalized toroidal flux $\sqrt{\psi/\psi_{\text{edge}}}$ for the optimized configuration (red line), W7-X (blue line) (Beidler *et al.* 2021) and LHD (green line) (Beidler *et al.* 2021).

as W7-X and the Large Helical Device (LHD) (Iiyoshi *et al.* 1990). The results are based on variational moments equilibrium code (VMEC) equilibria with 49 flux surfaces. We observe that $\epsilon_{\text{eff}}^{3/2}$ of CSSC is comparable to that of W7-X and is much smaller than that of LHD.

The other important target of optimization is the magnetic well which is a key parameter for MHD stability. The magnetic well is usually defined via the surface-averaged magnetic
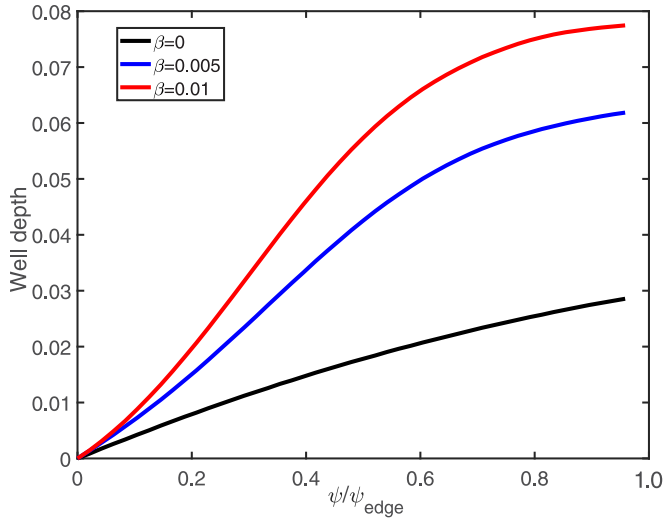
FIGURE 5. Magnetic well depth W versus the normalized toroidal flux ψ/ψ_{edge} for three values of plasma β.

pressure (Freidberg 2014) as

$$W = 2\frac{V}{\langle B^2 \rangle}\frac{\mathrm{d}}{\mathrm{d}V}\left\langle \frac{B^2}{2} \right\rangle, \tag{2.2}$$

where B is the magnetic field strength and $V(\psi)$ is the volume within flux surface ψ. A positive gradient of the surface-averaged magnetic field corresponds to a magnetic well. Figure 5 shows the magnetic well profile of CSSC for several plasma beta values. The results are based on free boundary equilibria obtained from the VMEC code. We see that the CSSC possesses a global magnetic well profile with well depth increasing with plasma beta. In addition to the magnetic well, we have also carried out initial MHD stability calculations using the 3-D MHD stability code TERPSICHORE (Anderson *et al.* 1990) to confirm a more complete MHD stability of the CSSC. The results show that low-n global MHD modes are stable up to the volume-averaged beta of $\beta = 1\,\%$. It should be noted that our optimization is done for a vacuum magnetic field. Future work will consider optimization at finite plasma beta.

So far, we have shown that the optimized configuration CSSC has both a magnetic well and low level of helical ripple. Now we show that these favourable properties are achieved with relatively simple coils, i.e. the shape of the two IL coils is relatively smooth with modest 3-D variation as compared to that of W7-X. Figure 6 compares the curvature of the IL coils of CSSC with that of one of W7-X's module coils at the same coil length of 1 m. We observe that the coil curvature of the CSSC is significantly smaller than that of the W7-X coil. Also, the variation of coil curvature along the coil loop is much less complex indicating that the coil complexity of the CSSC is much less in comparison.

3. Optimization methods

As described above, our optimization targets include plasma volume, rotational transform, flux surface quality, the effective helical ripple and the magnetic well. Below we describe some details of target evaluations and the optimization methods used in obtaining the CSSC.
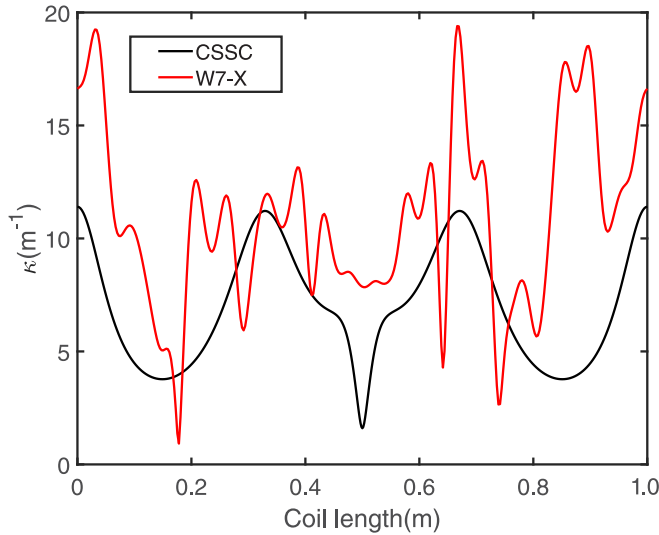
FIGURE 6. Coil curvature κ variation along the loop of coil for the optimized configuration (black line) and W7-X (red).

For each coil configuration, the optimization targets are evaluated based on the magnetic field generated by current-carrying coils. The magnetic field is calculated from the Biot–Savart law using the standard piecewise linear approach (Hanson & Hirshman 2002) for the integration along the coil loop. Each coil is divided into 720 segments in the integration. This number of segments is sufficient for obtaining accurate results of the magnetic field. After this work was completed, we became aware of a more efficient method of field calculation using the shifted piecewise linear approach (McGreivy *et al.* 2021). This better method will be used in our future work.

Based on above calculation of the magnetic field, the magnetic flux surfaces can be generated by tracing magnetic field lines. The field lines are traced starting from the points on the R-axis at $Z = 0$ and $\phi = 0$. First, the magnetic axis is located by requiring the field line returns to its starting point after one toroidal transit. Second, the magnetic flux surfaces are calculated by following field lines for many toroidal transits. Typically, up to 500 toroidal transits are used. For each field line, the intersection points of the field line with a poloidal plane (e.g. the $\phi = 0$ plane) form the 2-D Poincaré plot of the magnetic surface on that poloidal plane. The LCFS is located by requiring that the field line is confined within a finite volume close to coils. In addition, we require that the LCFS is not part of a magnetic island. We determine whether this condition is satisfied by inspecting the distribution of the intersection points. The intersection points are distributed very unevenly in poloidal angle for a magnetic island. If the difference of poloidal angle between two neighbouring points exceeds a threshold, the field line is judged to be part of a magnetic island and is not the LCFS. Then we search inward incrementally in the radial direction until the LCFS is located. The plasma volume within the LCFS can be calculated easily by integration in cylindrical coordinates. Third, the magnetic flux surfaces can be generated straightforwardly between the magnetic axis and the LCFS by field line tracing from a set of starting points between the magnetic axis and the LCFS. The flux surface quality is determined by inspecting the existence and width of magnetic islands within the LCFS. The flux surface quality is judged to be good if the sum of the island width is less than 10 % of the minor radius.

The rotational transform on each flux surface can be calculated by integrating along a field line on the surface. We use the rotational transform of the LCFS as one of our targets. Furthermore, the magnetic well can be evaluated based on (2.2) in principle by calculating the plasma volume and the averaged magnetic pressure on each flux surface. However, for simplicity, we just evaluate the flux surface-averaged magnetic field on two selected surfaces, namely the averaged field $\langle B_{\mathrm{LCFS}} \rangle$ on the LCFS and $\langle B_1 \rangle$ on the surface 1 cm away from the magnetic axis at the $\phi = 0$ plane. The difference $\delta B = \langle B_{\mathrm{LCFS}} \rangle - \langle B_1 \rangle$ is used as a proxy for the magnetic well. The configuration is judged to posses a global magnetic well if $\delta B > 0$. Finally, the effective helical ripple on a magnetic surface is calculated by integrating along a magnetic field line (Nemov *et al.* 1999), as was done in our recent work (Yu *et al.* 2021). We use the effective ripple coefficient on the LCFS as the target for neoclassical transport.

Now we describe some details of the optimization methods used. We vary the shape of the two IL coils via the ten Fourier coefficients as described above to search for desirable configurations that meet our targets. Since the total degrees of freedom is not a small number, a multi-stage random search algorithm is adopted in the optimization process. Specifically, at the first stage, the initial ranges of each degree of freedom are selected, as given in table 1. It should be noted that the range of each Fourier coefficient is constrained to be smaller for higher n to keep the coil complexity low. Given the ranges of parameters, a large collection of stellarator configurations are generated in the 12-dimensional parameter space with the value of each parameter randomly selected within its range. For the first stage, a total of 80 million cases are evaluated. A few good configurations are found that meet the criteria of $\epsilon_{\mathrm{eff}}^{3/2} < 0.01$ and $\iota > 0.2$ of the LCFS, plasma volume $V > 0.25 m^3$ and having a global magnetic well profile. This concludes the first stage of the search. At the second stage, this random search process is repeated starting from each of the good configurations found in the first stage. The ranges of parameters are updated based on each new configuration and are chosen to be narrower than those of the first stage. A total of four such stages of search were carried out in arriving at the final optimized configuration CSSC as defined in table 1. It should be noted that there are other optimized configurations with comparable quality. The details of other configurations will be given in another paper.

Finally, we discuss briefly about the choice of our optimization method used above. This global search method is appropriate because it maximizes the probability of finding the global optimum based on our targets. This global optimization method is also feasible because the number of free parameters is modest. Of course this method is not the most efficient and is computationally intensive. Other methods, such as Genetic Algorithm (Mitchell 2011) and Differential Evolution (Rocca, Oliveri & Massa 2011), are probably faster in finding optimized solutions. However, we believe that our method is more global and more capable of finding the globally optimized configuration.

4. Finite beta effects

In above calculation of global MHD stability at finite beta using TERPSICHORE, the free boundary equilibria are calculated using VMEC with bootstrap currents. A radial resolution of 49 flux surfaces is used in the VMEC calculations. The bootstrap currents are calculated with the SFINCS code. SFINCS is a kinetic code for the calculation of neoclassical transport in stellarators by solving the steady-state drift-kinetic equation for multiple species (Landreman *et al.* 2014). The pressure profile is chosen to be $p = p_0(1 - s^2)^3$ as shown in figure 7(*a*) for two values of the volume-averaged plasma beta β, where p_0 is the peak value and $s = \psi/\psi_{\mathrm{edge}}$ is the normalized toroidal flux. The temperature profile is chosen to be uniform and the density profile is the same
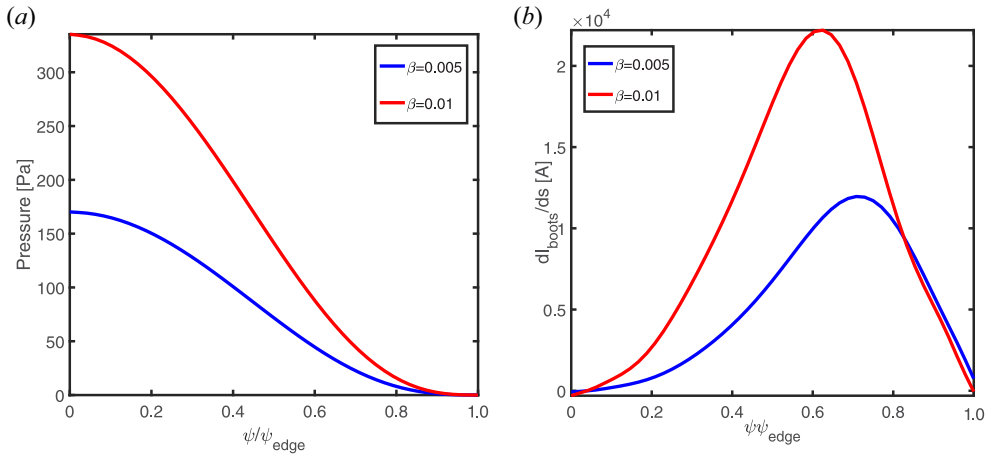
(*a*)

(*b*)

FIGURE 7. Pressure profiles in VMEC equilibriums and corresponding bootstrap current profiles calculated by SFINCS: (*a*) pressure profiles; (*b*) bootstrap current profiles.
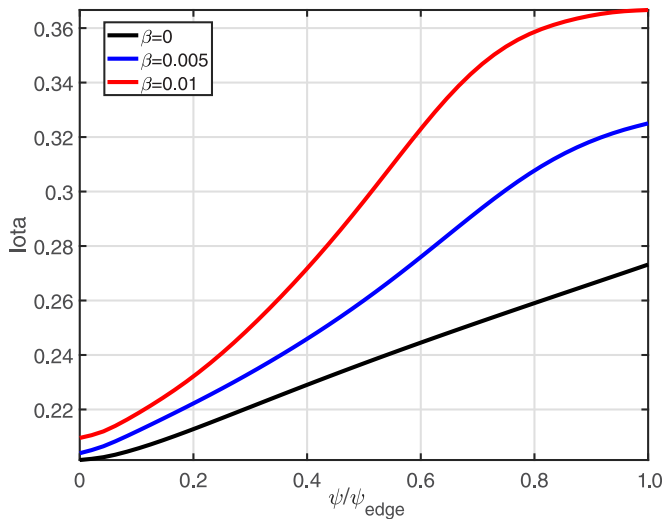

FIGURE 8. Rotational transform profiles for several values of plasma beta.

as the pressure profile. The peak electron and ion density is $n_{e0} = n_{i0} = 1 \times 10^{19}\,\mathrm{m}^{-3}$. The peak electron and ion temperatures are $T_{e0} = T_{i0} = 60\,\mathrm{eV}$ for $\beta = 0.005$ and $T_{e0} = T_{i0} = 120\,\mathrm{eV}$ for $\beta = 0.01$. The volume averaged magnetic field is $\langle B \rangle = 0.2T$. The self-consistent bootstrap current profiles in finite beta equilibria are obtained using the iterative method. Specifically, the initial bootstrap current profile is calculated using the zero beta equilibrium. Then the equilibrium at a finite beta is calculated iteratively with updated bootstrap current profiles. A converged bootstrap profile can usually be obtained after several iterations. The final converged bootstrap current profiles are shown in figure 7(*b*).

Figure 8 shows the iota profile at several values of plasma beta. We observe that the iota profile increases as beta increases due to bootstrap current and the edge iota value increases approximately 30 % from the vacuum value at $\beta = 0.01$. Furthermore, the effects
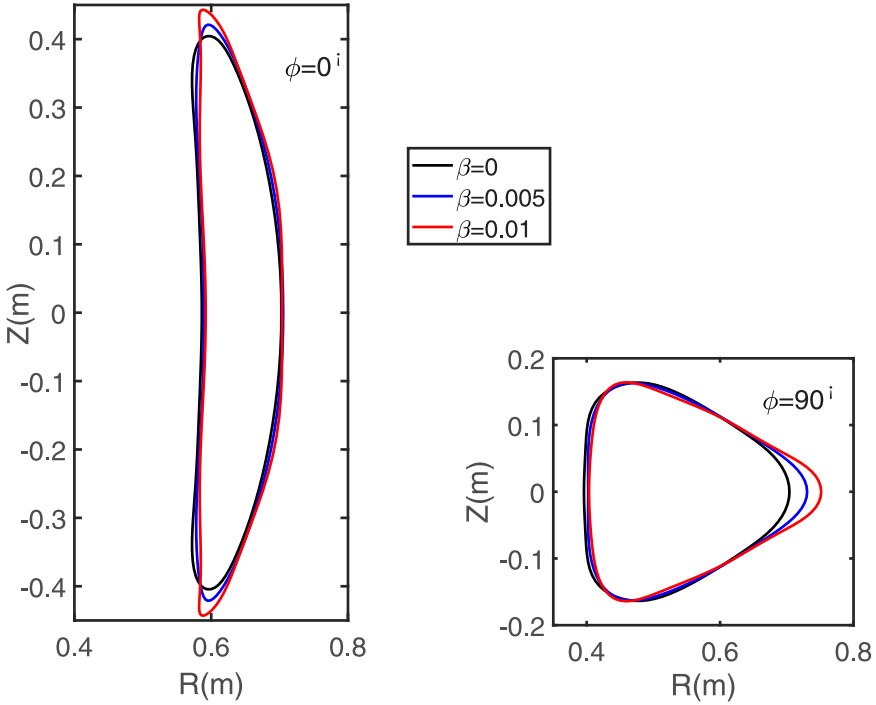
FIGURE 9. Free boundary flux surfaces at $\phi = 0°$ and $\phi = 90°$ with the same toroidal magnetic flux for several values of plasma beta.
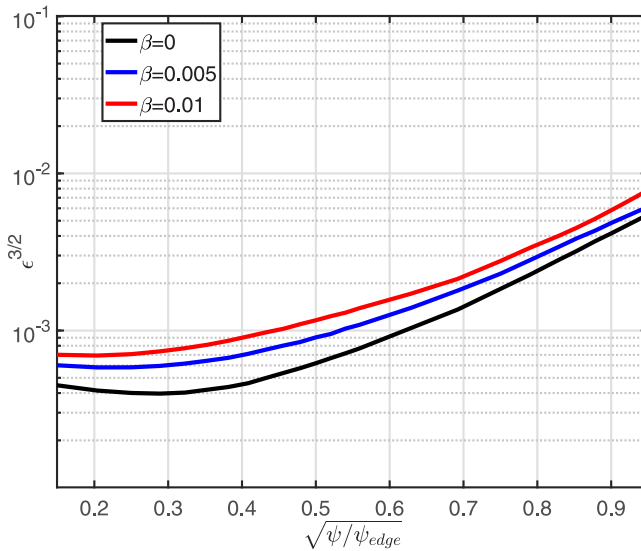

FIGURE 10. Effective ripple profiles for several values of plasma beta.

of finite beta also modify the shape of the plasma boundary as expected. Figure 9 shows the last closed flux surfaces for several beta values. The plasma boundary shape is seen to vary quite a bit as the beta value increases. Correspondingly, the effective helical ripple increases with beta as shown in figure 10. This result is not too surprising since our

optimization is done at zero beta. Future work will take into account the important effects of finite beta.

5. Conclusions

In conclusion, a direct optimization from coils demonstrates the existence of a new optimized stellarator with four simple coils. The optimized configuration has favourable properties of a magnetic well and a low effective helical ripple level comparable to that of W7-X. The two interlocking coils have a much simpler smooth 3-D shape when compared to those of advanced stellarators such as W7-X. This work opens up possibilities of future stellarator reactors with simplified coils. In the near term, the optimized configuration can be used as a basis for a low-cost experimental device to study the MHD stability and plasma confinement of compact stellarators. The design could also be used as a candidate stellarator for electron–positron plasma experiments.

Declaration of interests

The authors report no conflict of interest.

REFERENCES

ANDERSON, D.V., COOPER, W.A., GRUBER, R., MERAZZI, S. & SCHWENN, U. 1990 Methods for the efficient calculation of the (MHD) magnetohydrodynamic stability properties of magnetically confined fusion plasmas. *Intl J. Supercomput. Applics.* **4** (3), 34–47.

BEIDLER, C.D., SMITH, H.M., ALONSO, A., ANDREEVA, T., BALDZUHN, J., BEURSKENS, M., BORCHARDT, M., BOZHENKOV, S.A., BRUNNER, K.J. & DAMM, H. 2021 Demonstration of reduced neoclassical energy transport in Wendelstein 7-X. *Nature* **596**, 221–226.

BOOZER, A.H. 2021 Stellarators as a fast path to fusion. *Nucl. Fusion* **61** (9), 096024.

DINKLAGE, A., BEIDLER, C.D., HELANDER, P., FUCHERT, G. & GIANNELLA, V. 2018 Magnetic configuration effects on the Wendelstein 7-X stellarator. *Nat. Phys.* **14** (8), 855–860.

FREIDBERG, J.P. 2014 *Ideal MHD*. Cambridge University Press.

HANSON, J.D. & HIRSHMAN, S.P. 2002 Compact expressions for the Biot–Savart fields of a filamentary segment. *Phys. Plasmas* **9** (10), 4410–4412.

HELANDER, P., DREVLAK, M., ZARNSTORFF, M. & COWLEY, S.C. 2020 Stellarators with permanent magnets. *Phys. Rev. Lett.* **124**, 095001.

HENNEBERG, S.A., HUDSON, S.R., PFEFFERLÉ, D. & HELANDER, P. 2021 Combined plasma–coil optimization algorithms. *J. Plasma Phys.* **87** (2), 905870226.

HO, D.D.-M. & KULSRUD, R.M. 1987 Neoclassical transport in stellarators. *Phys. Fluids* **30** (2), 442–461.

IIYOSHI, A., FUJIWARA, M., MOTOJIMA, O., OHYABU, N. & YAMAZAKI, K. 1990 Design study for the large helical device. *Fusion Technol.* **17** (1), 169–187.

KRUGER, T.G., ZHU, C.X., BADER, A., ANDERSON, D.T. & SINGH, L. 2021 Constrained stellarator coil curvature optimization with FOCUS. *J. Plasma Phys.* **87** (2), 175870201.

LANDREMAN, M., SMITH, H.M., MOLLÉN, A. & HELANDER, P. 2014 Comparison of particle trajectories and collision operators for collisional transport in nonaxisymmetric plasmas. *Phys. Plasmas* **21** (4), 042503.

LOBSIEN, J.F., DREVLAK, M. & PEDERSEN, T.S. 2018 Stellarator coil optimization towards higher engineering tolerances. *Nucl. Fusion* **58** (10), 106013.

MCGREIVY, N., ZHU, C., GUNDERSON, L.M. & HUDSON, S.R. 2021 Computation of the Biot–Savart line integral with higher-order convergence using straight segments. *Phys. Plasmas* **28** (8), 082111.

MITCHELL, M. 2011 *An Introduction to Genetic Algorithms*. MIT Press.

NEILSON, G.H., GRUBER, C.O., HARRIS, J.H., REJ, D.J., SIMMONS, R.T. & STRYKOWSKY, R.L. 2010 Lessons learned in risk management on NCSX. *IEEE Trans. Plasma Sci.* **38** (3), 320–327.

NEMOV, V.V., KASILOV, S.V., KERNBICHLER, W. & HEYN, M.F. 1999 Evaluation of $1/\nu$ neoclassical transport in stellarators. *Phys. Plasmas* **6** (12), 4622–4632.

PEDERSEN, T.S., DANIELSON, J.R., HUGENSCHMIDT, C., MARX, G., SARASOLA, X., SCHAUER, F., SCHWEIKHARD, L., SURKO, C.M. & WINKLER, E. 2012 Plans for the creation and studies of electron–positron plasmas in a stellarator. *New J. Phys.* **14** (3), 035010.

RIßE, K. 2009 Experiences from design and production of Wendelstein 7-X magnets. *Fusion Engng Des.* **84** (7), 1619–1622, proceeding of the 25th Symposium on Fusion Technology.

ROCCA, P., OLIVERI, G. & MASSA, A. 2011 Differential evolution as applied to electromagnetics. *IEEE Antennas Propag. Mag.* **53** (1), 38–49.

WOLF, R.C., ALI, A., ALONSO, A., BALDZUHN, J., BEIDLER, C., BEURSKENS, M., BIEDERMANN, C., BOSCH, H.-S., BOZHENKOV, S., BRAKEL, R., *et al.* 2017 Major results from the first plasma campaign of the Wendelstein 7-X stellarator. *Nucl. Fusion* **57** (10), 102020.

XU, G.S., LU, Z.Y., CHEN, D.H., CHEN, L., ZHANG, X.Y., WU, X.Q., YE, M.Y. & WAN, B.N. 2021 Design of quasi-axisymmetric stellarators with varying-thickness permanent magnets based on Fourier and surface magnetic charges method. *Nucl. Fusion* **61** (2), 026025.

YU, G.D., FENG, Z.C., JIANG, P.Y., POMPHREY, N., LANDREMAN, M. & FU, G.Y. 2021 A neoclassically optimized compact stellarator with four planar coils. *Phys. Plasmas* **28** (9), 092501.

ZHU, C.X., HUDSON, S.R., SONG, Y.T. & WAN, Y.X. 2017 New method to design stellarator coils without the winding surface. *Nucl. Fusion* **58** (1), 016008.

ZHU, C.X., ZARNSTORFF, M., GATES, D. & BROOKS, A. 2020 Designing stellarators using perpendicular permanent magnets. *Nucl. Fusion* **60** (7), 076016.